• Basic Research •

Hypoxia-activated microglia promote pathological angiogenesis *via* an FN/ITGB3/FAK/Akt pathway

Lan-Cao Hao[1], De-Hui Li[2], Kun Zhang[3], Chen-Zi Liu[4], Ming-Hao Sun[5], Xin-Xiao Gao[1], Si-Quan Zhu[1,5]

[1]Department of Ophthalmology, Beijing Anzhen Hospital, Capital Medical University, Beijing 100029, China
[2]Beijing Collaborative Innovation Centre for Cardiovascular Disorders, the Key Laboratory of Remodeling-Related Cardiovascular Disease, Ministry of Education, Beijing Anzhen Hospital, Capital Medical University, Beijing 100029, China
[3]Department of Vascular Surgery, Beijing Luhe Hospital, Capital Medical University, Beijing 101100, China
[4]Department of Ophthalmology, Wangjing Hospital, China Academy of Chinese Medical Sciences, Beijing 100102, China
[5]Xiamen Eye Center and Eye Institute of Xiamen University, School of Medicine, Xiamen University, Xiamen 361004, Fujian Province, China
Correspondence to: Si-Quan Zhu. Department of Ophthalmology, Beijing Anzhen Hospital, Capital Medical University, No.2 Anzhen Road, Chaoyang District, Beijing 100029, China. siquanzhu@sina.com
Received: 2026-01-20 Accepted: 2026-07-07

Abstract

● **AIM:** To investigate whether hypoxia-activated microglia drive pathological neovascularization through extracellular matrix (ECM) remodeling and endothelial integrin signaling, a mechanism that may function in parallel with vascular endothelial growth factor (VEGF) signaling.

● **METHODS:** The oxygen-induced retinopathy (OIR) mouse model was used. Retinal phenotypes were assessed by flat mounts, histology, and vascular leakage assays. Key pathways were screened by transcriptomics and validated *via* Western blot, immunofluorescence, and quantitative polymerase chain reaction (qPCR). *In vitro*, brain microvascular endothelial cells were treated with conditioned medium from hypoxic microglia (Hyp-CM), with cell migration and tube formation assessed. Interventions employed the integrin β3 (ITGB3) inhibitor cilengitide, the focal adhesion kinase (FAK) inhibitor PF-573228 and a neutralizing anti-VEGF antibody. *In vivo*, cilengitide was administered by intravitreal injection to evaluate its therapeutic effect on neovascularization.

● **RESULTS:** OIR retinas showed significant avascularity, pathological neovascularization, and barrier disruption. Transcriptomics revealed activation of ECM-receptor interaction and focal adhesion pathways, with upregulation of *Fn1* and *Itgb3*. Increased protein levels of fibronectin (FN) and ITGB3, alongside elevated phosphorylation of FAK and protein kinase B (Akt), were confirmed *in vivo*. Activated microglia co-localized with upregulated FN and ITGB3. Conditioned medium from Hyp-CM activated the ITGB3-FAK-Akt pathway in endothelial cells and promoted their migration and tube formation. These effects were nearly abolished by cilengitide or PF-573228. VEGF neutralization partially reduced Hyp-CM-induced migration and tube formation. Intravitreal injection of cilengitide significantly reduced retinal neovascularization in OIR mice.

● **CONCLUSION:** Hypoxia-activated microglia promote pathological angiogenesis, and the FN/ITGB3/FAK/Akt axis is identified as a key mediator of this process, revealing a novel mechanism that operates in parallel with VEGF signaling. Targeting this "hypoxia-microglia-ECM-integrin" axis represents a promising therapeutic strategy to overcome anti-VEGF resistance in ischemic retinopathy.

● **KEYWORDS:** oxygen-induced retinopathy; pathological neovascularization; microglia; extracellular matrix; integrin β3; focal adhesion kinase

DOI:10.18240/ijo.2026.11.02

Citation: Hao LC, Li DH, Zhang K, Liu CZ, Sun MH, Gao XX, Zhu SQ. Hypoxia-activated microglia promote pathological angiogenesis *via* an FN/ITGB3/FAK/Akt pathway. *Int J Ophthalmol* 2026;19(11):2098-2111

INTRODUCTION

Pathological retinal neovascularization (RNV), a final common pathway in diseases like retinopathy of prematurity (ROP) and diabetic retinopathy, is a leading cause of global blindness[1-2]. The current standard of care relies on therapies targeting vascular endothelial growth factor (VEGF). However, a significant proportion of patients exhibit an incomplete or diminishing response over time, characterized

by persistent vascular leakage and fibrosis, highlighting the critical clinical problem of anti-VEGF resistance[3-5]. This stark reality underscores an urgent need to identify alternative mechanisms that bypass VEGF signaling to drive therapy-resistant neovascularization.

The research focus has shifted from a singular growth factor model to the dysregulated microenvironment of the neurovascular unit. Within this framework, microglia—the resident immune cells of the retina—have emerged as key players. In ischemia, they rapidly activate and aggregate near new vessels, a state correlated with pathological angiogenesis[6]. Crucially, activated microglia are active remodelers of their surroundings, capable of altering the composition and mechanics of the extracellular matrix (ECM)[2,7]. A hallmark of this pathological ECM remodeling is the upregulation of fibronectin (FN). FN engages its high-affinity receptor, integrin β3 (ITGB3), on endothelial cells, triggering outside-in signaling that activates focal adhesion kinase (FAK) and protein kinase B (Akt), a well-defined pathway governing cell adhesion, migration, and survival[8-10]. Notably, this FN-ITGB3-FAK/Akt axis is recognized as a mechanotransduction pathway, recently implicated in ocular fibrotic diseases[11]. This provides a compelling precedent for its role in transducing microenvironmental changes into pro-angiogenic signals.

Despite these advances, a critical gap persists in ischemic retinopathy. While hypoxia is the primary driver, and microglia and integrin signaling are implicated, it remains unclear whether and how hypoxic stress orchestrates these elements into a coherent pathway that can function independently of, or in parallel with, VEGF signaling. While hypoxia-activated microglia and integrin signaling have been individually implicated, the complete axis linking hypoxic microglia to FN-rich ECM remodeling and subsequent ITGB3/FAK/Akt activation remains untested.

To address this, we proposed the central hypothesis that a hypoxia-driven "microglia–ECM–integrin" axis fuels VEGF-resistant neovascularization. Using the oxygen-induced retinopathy (OIR) mouse model, we combined transcriptomic screening, *in vivo* validation, and *in vitro* functional assays with specific pharmacological inhibitors (Cilengitide for β3, PF-573228 for FAK).

MATERIALS AND METHODS

Ethical Approval All animal experiments were approved by the Experimental Animal Welfare and Ethics Committee of Beijing Institute of Cardiopulmonary Vascular Disease/Beijing Anzhen Hospital Affiliated to Capital Medical University (Approval No. AZ2025LA030).

Oxygen-Induced Retinopathy Model C57BL/6J mice were housed under specific pathogen-free conditions with a 12h/12h light/dark cycle. Mice were assigned to either the normal control (Ctrl) group or the OIR group. The OIR model was established as described previously[12-13]. Briefly, on postnatal day (P) 7, pups and their nursing dam were placed in a high-oxygen environment (75%±2%) for 5d until P12, and then returned to room air (21% oxygen) until P17. Ctrl pups were maintained in room air throughout. At P17, mice were euthanized under isoflurane anesthesia, and eyeballs were enucleated for analysis. Sample sizes are indicated for each assay below.

For *in vivo* pharmacological inhibition, OIR mice at P12 received an intravitreal injection of 0.5 μL of cilengitide (10 μmol/L, Selleck, S6387) in the right eye, and the left eye received an equal volume of isotype control immunoglobulin G (IgG; 10 μg/mL, R&D Systems, AB-108-C) as a negative control. Injections were performed under a dissecting microscope using a 33-gauge needle (Hamilton). At P17, retinas were harvested for platelet endothelial cell adhesion molecule-1 (CD31) staining and quantification of the neovascular area.

Retinal Whole Mount and Immunofluorescence Staining Eyeballs were fixed in 4% paraformaldehyde for 1h. Retinas were dissected to prepare whole mounts, permeabilized with 0.5% Triton X-100, and blocked with 5% bovine serum albumin (BSA). They were incubated overnight at 4°C with a primary antibody against CD31 (1:300, Servicebio, GB113151), followed by a corresponding secondary antibody (1:300, Servicebio, GB21303) for 2h at room temperature. Images were acquired using a confocal microscope. The avascular area and RNV area were measured using ImageJ software and expressed as a percentage of the total retinal area (n=8 mice per group).

Retinal Histology and Hematoxylin and Eosin Staining Eyes were fixed, embedded in paraffin, and sectioned sagittally at 5 μm thickness. Sections were stained with hematoxylin and eosin (H&E). After whole-slide scanning, all endothelial cell nuclei breaching the internal limiting membrane were counted on each section (n=8 mice per group).

Assessment of Vascular Leakage At P17, mice were intravenously injected with 20 mg/mL fluorescein isothiocyanate (FITC)-dextran (70 kDa, FD70S, Sigma-Aldrich, 60842-46-8). After 30min, mice were perfused with phosphate buffered saline (PBS). Retinal whole mounts were prepared, sealed, and immediately imaged using a fluorescence microscope (Nikon ECLIPSE Ni, Japan). Extravascular fluorescence intensity was quantified using ImageJ (n=8 mice per group).

Transcriptomic Sequencing and Bioinformatic Analysis Total RNA was extracted from retinal tissues using TRIzol reagent (Invitrogen, 15596026CN). Sequencing libraries were prepared by Novogene. mRNA was purified using poly-T oligo-attached magnetic beads, followed by fragmentation,

cDNA synthesis, end repair, adapter ligation, and polymerase chain reaction (PCR) amplification. After quality control, strand-specific RNA sequencing was performed on an Illumina NovaSeq platform. Raw reads were processed with Fastp and aligned to the mouse reference genome using HISAT2 (v2.0.5). Differentially expressed genes (DEGs) were identified using DESeq2 with the following criteria: $|\log_2\text{FoldChange}|>1$ and adjusted *P*-value (*P*adj)<0.05. Gene Ontology (GO) and Kyoto Encyclopedia of Genes and Genomes (KEGG) pathway enrichment analyses for upregulated DEGs were performed using the clusterProfiler R package. Three biological replicates were included per group, each consisting of a pool of 4 retinas.

Quantitative Real-Time PCR Total RNA was extracted from retinal tissues using FreeZol Reagent (Vazyme, R711-01). RNA concentration and purity were assessed using a NanoDrop 2000 (Thermo Fisher Scientific, USA). cDNA was synthesized from total RNA using ABScript Neo RT Master Mix (ABclonal Technology, RK20433) on a PCR instrument (BIOER, China). Quantitative polymerase chain reaction (qPCR) was performed using a SYBR Green qPCR kit (Abclonal, RK21203) on a QuantStudio 1 system (Thermo Fisher Scientific, USA). The *Rplp0* gene was validated to be stably expressed across all experimental groups and was used as the internal reference gene. Relative mRNA expression levels were calculated using the $2^{-\Delta\Delta Ct}$ method (*n*=8 independent retinal samples per group).

Western Blot Analysis Proteins were extracted from cells or tissues using RIPA lysis buffer (Solarbio, R0010). Protein concentration was determined using a BCA protein assay kit (Thermo Fisher Scientific, 23225). Equal amounts of protein, along with a prestained protein molecular weight marker (10–250 kDa, Thermo Fisher Scientific, 26619), were separated by sodium dodecyl sulfate-polyacrylamide gel electrophoresis (SDS-PAGE) and transferred to polyvinylidene difluoride (PVDF) membranes (Millipore, ISEQ00010). Membranes were incubated overnight (approximately 16–18h) at 4°C with the following primary antibodies: anti-FN (1:500, Proteintech, 15613-1-AP), anti-ITGB3 (1:1000, Abcam, Ab119992), anti-FAK (1:50 000, Proteintech, 12636-1-AP), anti-phospho-FAK (Tyr397; 1:1000, Abcam, ab81298), anti-Akt (1:1000, Cell Signaling Technology, 4691S), anti-phospho-Akt (Ser473; 1:2000, Cell Signaling Technology, 4060S), and anti-β-actin (1:50 000, Abclonal, AC038). Membranes were then incubated with appropriate fluorescent secondary antibodies (1:40 000, LI-COR, 926-32211) at room temperature for 1h. Fluorescence scanning was performed using a dual-color infrared laser imaging system (LI-COR Odyssey Sa, USA), and band intensities were quantified using ImageJ software (*n*=3 independent biological replicates). For re-probing, antibodies were stripped from the PVDF membranes using stripping buffer (Solarbio, SW3020).

Immunofluorescence Co-Staining on Retinal Sections Retinal paraffin sections were dewaxed, subjected to antigen retrieval, and blocked. Sections were then incubated overnight at 4°C with primary antibodies: anti-CD31 (1:300, Servicebio, GB15063), anti-FN (1:100, Proteintech, 15613-1-AP), anti-ITGB3 (1:200, Abcam, Ab119992), anti-Iba1 (1:200, Wako, 019-19741), and anti-CD86 (1:1000, Servicebio, GB150054). This was followed by incubation with appropriate fluorescent secondary antibodies (1:1000, Beyotime) and 4',6-diamidino-2-phenylindole (DAPI). Images were acquired using a confocal microscope (OLYMPUS FV3000-OSR, Japan; *n*=8 mice per group).

For microglial morphology analysis, Iba1+cells were examined in four randomly selected fields per retina (*n*=8 mice per group). Cells with a clearly identifiable cell body were counted and classified as ramified (small soma, fine processes) or amoeboid (activated; enlarged soma, thickened/shortened processes). The proportion of activated microglia was calculated as (number of amoeboid cells/total Iba1+cells)×100%.

For quantitative co-localization analysis, Manders' coefficients (M1 for ITGB3 overlapping CD31, M2 for CD31 overlapping ITGB3) were calculated using the JACoP plugin (ImageJ) with Costes' automatic thresholding to exclude background noise.

Cell Culture The BV2 mouse microglial cell line (purchased from the Chinese Academy of Sciences Cell Bank/Stem Cell Bank) and the BEnd.3 mouse brain microvascular endothelial cell line (purchased from the Bowers Type Culture Collection) were cultured in Dulbecco's Modified Eagle's Medium (DMEM, Gibco, 10566016) supplemented with 10% fetal bovine serum (Corning, 35-179-CV), 100 U/mL penicillin, and 100 μg/mL streptomycin (Thermo Fisher Scientific, 15140122). Cells were maintained at 37°C in a normoxic incubator with 5% CO_2.

Preparation of Microglial Conditioned Medium To investigate microglia-endothelial cell communication, BV2 cells were seeded in 6-well plates. When cell density reached approximately 70%, the medium was replaced with fresh complete medium. The experimental group was then transferred to a hypoxic incubator (1% O_2, 5% CO_2) for 24h, while the control group remained under normoxic conditions. After incubation, the supernatant was collected, centrifuged to remove cell debris, and used as conditioned medium (CM). BEnd.3 cells were divided into three treatment groups: Ctrl (cultured in complete medium), normoxic conditioned medium group (Ctrl-CM, cultured in CM from normoxic BV2 cells), and hypoxic conditioned medium group (Hyp-CM, cultured in CM from hypoxic BV2 cells).

Pharmacological and Inhibitor Treatments For pharmacological intervention experiments, BEnd.3 cells were divided into six groups: Ctrl, dimethyl sulfoxide (DMSO)

vehicle control (Ctrl+DMSO), recombinant FN protein stimulation (Ctrl+FN), Hyp-CM, Hyp-CM plus cilengitide (Hyp-CM+Cil), and Hyp-CM plus PF-573228 (Hyp-CM+PF). Inhibitors were dissolved in DMSO as stock solutions. An equivalent volume of DMSO was added to the Ctrl+DMSO group to ensure a consistent final DMSO concentration across all treatment groups, not exceeding 0.1% (v/v). The Ctrl+FN group was stimulated by adding 50 μg/mL recombinant FN protein (ZYBio, ZY60020MuP) to the complete medium. The Hyp-CM+Cil and Hyp-CM+PF groups were treated with Hyp-CM supplemented with 10 μmol/L of the integrin αvβ3/αvβ5 inhibitor cilengitide (Selleck, S6387) or the FAK inhibitor PF-573228 (Selleck, S2013), respectively.

VEGF Neutralization Experiment To determine whether VEGF contributes to the pro-angiogenic effects of Hyp-CM, neutralizing anti-mouse VEGF antibody (αVEGF, R&D Systems, AF-493-NA) and recombinant mouse VEGF 164 Protein (rmVEGF, R&D Systems, 493-MV) were used. BEnd.3 cells were treated with the following conditions: Ctrl (basal medium), Hyp-CM, Hyp-CM+IgG (10 μg/mL isotype control), Hyp-CM+αVEGF (10 μg/mL αVEGF), and rmVEGF+αVEGF (10 ng/mL rmVEGF plus 10 μg/mL αVEGF as a positive control for antibody neutralization). All treatments were applied in both scratch wound healing and tube formation assays. The isotype control IgG group was included to rule out non-specific effects of the antibody.

Scratch Wound Healing Assay Three parallel lines were pre-marked on the back of 12-well plates for field positioning. BEnd.3 cells were seeded at a density of 2×10^5 cells per well. After approximately 24h of culture, when cells reached near confluence, a straight wound was created using a 200 μL sterile pipette tip perpendicular to the marked lines. The wells were gently washed with PBS 1–2 times to remove detached cells and then replenished with the respective treatment media. Images of the same fields were captured at 0, 12, 24, and 48h after scratching using an inverted biological microscope (OLYMPUS CKX53, Japan). The wound healing rate was calculated using ImageJ software (n=3 independent experiments).

Endothelial Tube Formation Assay Matrigel matrix (Corning, 356237) was thawed overnight at 4°C. Using pre-cooled pipette tips and keeping all materials on ice, 10 μL of Matrigel was added to each well of a μ-Slide Angiogenesis 15-well plate (Ibidi, 81506). The plate was then transferred to a 37°C incubator for 30–60min to allow polymerization. BEnd.3 cells were resuspended in different treatment media and seeded onto the Matrigel at a density of 1×10^4 cells per well. After 6h of incubation at 37°C, images were captured using an inverted biological microscope (OLYMPUS CKX53, Japan). Tube formation was assessed by quantifying the number of tube network nodes and total branch length using the Angiogenesis Analyzer plugin for ImageJ (n=3 independent experiments).

Statistical Analysis All statistical analyses were performed using GraphPad Prism software (version 10.1.2, GraphPad Software Inc., USA). Data are presented as mean±standard deviation (SD). Comparisons between two groups were made using an unpaired two-tailed Student's t-test. Comparisons among multiple groups were performed using one-way analysis of variance (ANOVA) followed by Tukey's post hoc test. Statistical significance was defined as $P<0.05$, $P<0.01$, $P<0.001$, $P<0.0001$. "ns" indicates not significant ($P>0.05$).

RESULTS

OIR Mouse Model Exhibits Pathological Neovascularization and Blood-Retinal Barrier Damage To investigate the pathogenesis of OIR, we established the OIR mouse model. Retinas from OIR mice at P17 exhibited significant pathological alterations compared to normoxic controls (experimental timeline in Figure 1A).

CD31 immunofluorescence staining of retinal whole mounts revealed a large central avascular area in OIR retinas, contrasting with the intact vascular network in controls (Figure 1B). The avascular area relative to the total retinal area was 13.85%±2.29% in the OIR group, compared to only 0.098%±0.089% in controls ($P<0.0001$; Figure 1C). To directly assess pathological angiogenesis, we quantified RNV area in the same retinal flat mounts. OIR retinas showed clustered, tortuous neovascular structures, which were absent in controls (Figure 1B). Quantitative analysis revealed that the neovascular area occupied 1.79%±0.29% of the total retinal area in OIR mice, while no neovascular tufts were detected in controls (Figure 1D; $P<0.0001$). Correlation analysis demonstrated a strong positive correlation between the avascular area and the neovascular area [Pearson r=0.8427, 95% confidence interval (CI): 0.3399–0.9709, P=0.0086], confirming that ischemia-driven vaso-obliteration directly correlates with subsequent pathological neovascularization. H&E-stained sections showed numerous endothelial cell nuclei breaching the internal limiting membrane in OIR retinas (Figure 1E), with a significantly higher count than in controls ($P<0.0001$; Figure 1F), indicating pathological neovessel formation. Vascular leakage assays demonstrated a significantly higher intensity of total fluorescence intensity (log10) in the OIR group ($P<0.0001$; Figure 1G, 1H), confirming blood-retinal barrier disruption.

Transcriptomic Screening Implicates ECM and Focal Adhesion Pathways Transcriptomic sequencing of P17 retinal tissues revealed 421 significantly upregulated and 87 downregulated genes in OIR versus control retinas (Figure 2A). Enrichment analysis of upregulated genes showed significant associations with ECM organization and focal adhesion pathways (Figure 2B, 2C). Intersection of the "focal adhesion" and "ECM-receptor interaction" pathways showed all common

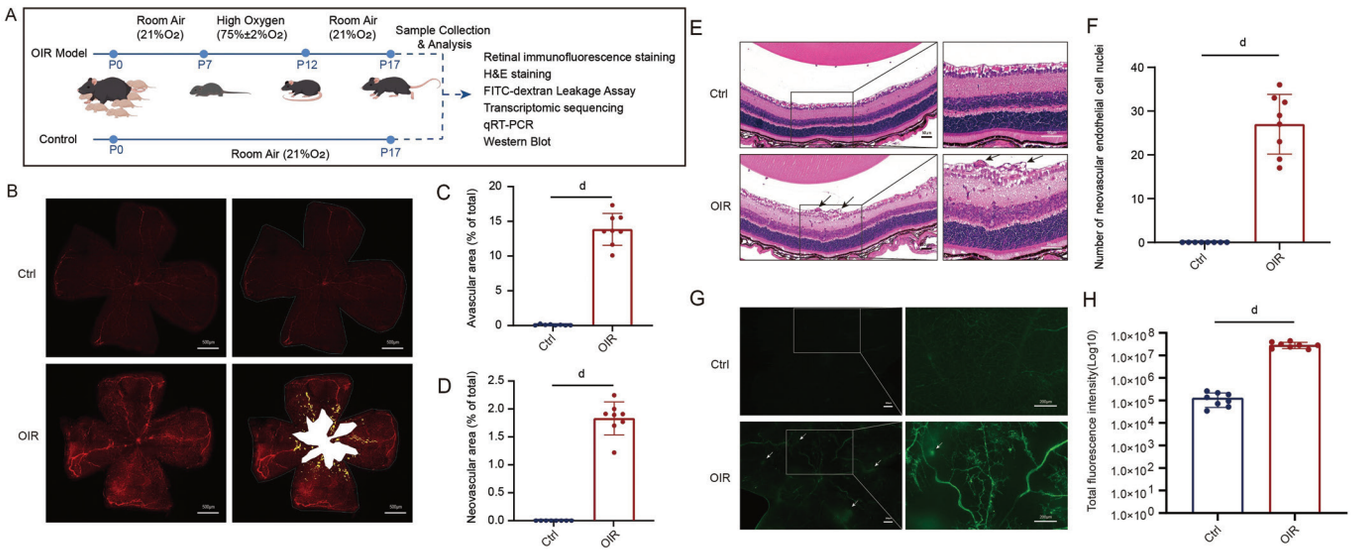


Figure 1 Pathological neovascularization and vascular leakage in the OIR mouse model Data are mean±SD. Statistical significance was determined by unpaired *t*-test: $^{d}P<0.0001$. A: Schematic flowchart of OIR mouse model establishment and phenotypic analysis (created with Figdraw); B: Representative CD31-immunostained retinal whole mounts from Ctrl and OIR mice at P17. The cyan dashed line outlines the entire retina. The white area indicates the central avascular zone, and the yellow areas indicate neovascular tufts. Scale bar: 500 μm; C: Quantitative analysis of the avascular area (% of total retinal area; *n*=8 mice per group); D: Quantitative analysis of the neovascular area (% of total retinal area; *n*=8 mice per group); E: Representative H&E-stained retinal sections. The left panel shows a field at 20-fold magnification, the right panel at 40-fold magnification. Black arrowheads indicate endothelial cell nuclei breaching the ILM. Scale bar: 50 μm; F: Quantification of endothelial cell nuclei breaching the ILM (*n*=8 mice per group); G: Representative images of retinal vascular leakage assessed by FITC-dextran (FD70S) angiography. The left panel shows a field at 4-fold magnification, the right panel at 10-fold magnification. White arrows indicate extravascular fluorescence leakage. Scale bar: 200 μm; H: Quantification of total fluorescence intensity (log10; *n*=8 mice per group). Ctrl: Control; OIR: Oxygen-induced retinopathy; P: Postnatal day; H&E: Hematoxylin and eosin; ILM: Internal limiting membrane; SD: Standard deviation; CD31: Platelet endothelial cell adhesion molecule-1; FITC: Fluorescein isothiocyanate; qRT-PCR: Quantitative reverse transcription polymerase chain reaction.

genes were differentially expressed in OIR (Figure 2D). Notably, *Fn1* and *Itgb3* were among the most prominently upregulated genes, a change validated by quantitative reverse transcription PCR (qRT-PCR) in independent samples (Figure 2E). These results indicate OIR pathology is closely linked to extensive activation of ECM remodeling and cell-matrix adhesion signaling.

***In vivo* Validation of FN-ITGB3-FAK/Akt Pathway Activation and Association with Activated Microglia**

Given that the KEGG pathway analysis showed significant enrichment of the focal adhesion pathway (Figure 2C), and that ITGB3 is known to activate FAK and its downstream effector Akt upon binding to ECM ligands such as FN, we next examined the protein levels and phosphorylation status of FAK and Akt in OIR retinas. Western blot analysis confirmed significant upregulation of FN and ITGB3 protein in OIR retinal tissues (FN: $P=0.0464$; ITGB3: $P=0.0004$; Figure 3A–3C). Phosphorylation levels of FAK and Akt were also significantly elevated (p-FAK: $P=0.0007$; p-Akt: $P=0.0002$; Figure 3E, 3H), as were their total protein levels (Figure 3D, 3G). The p-FAK/FAK and p-Akt/Akt ratio was significantly increased (p-FAK/FAK: $P=0.0149$; p-Akt/Akt: $P=0.0078$; Figure 3F, 3I), indicating enhanced FAK and Akt activity.

Immunofluorescence staining showed significantly enhanced expression of the microglial markers Iba1 ($P<0.0001$) and CD86 ($P<0.0001$) in OIR retinas, with activated microglia co-localizing with CD31+endothelial cells in neovascular clusters (Figure 3J–3L). In control retinas, Iba1+cells exhibited ramified morphology, whereas OIR retinas showed predominantly amoeboid (activated) morphology (enlarged somata, thickened/shortened processes). Quantification confirmed that the proportion of activated microglia was significantly higher in OIR mice (65.48%±4.88% *vs* 6.29%±1.68%, $P<0.0001$, Figure 3M), corroborating the increased Iba1/CD86 fluorescence intensity.

Concurrently, FN and ITGB3 expression was upregulated (FN: $P<0.0001$; ITGB3: $P<0.0001$) and showed co-localization in neovascular areas (Figure 3N–3P). Quantitative co-localization analysis using Manders' coefficients with Costes' automatic thresholding revealed that, in OIR retinas, ITGB3 signal overlapped with $CD31^{+}$ endothelial cells at M1=0.962±0.031, and CD31 signal overlapped with $ITGB3^{+}$ areas at

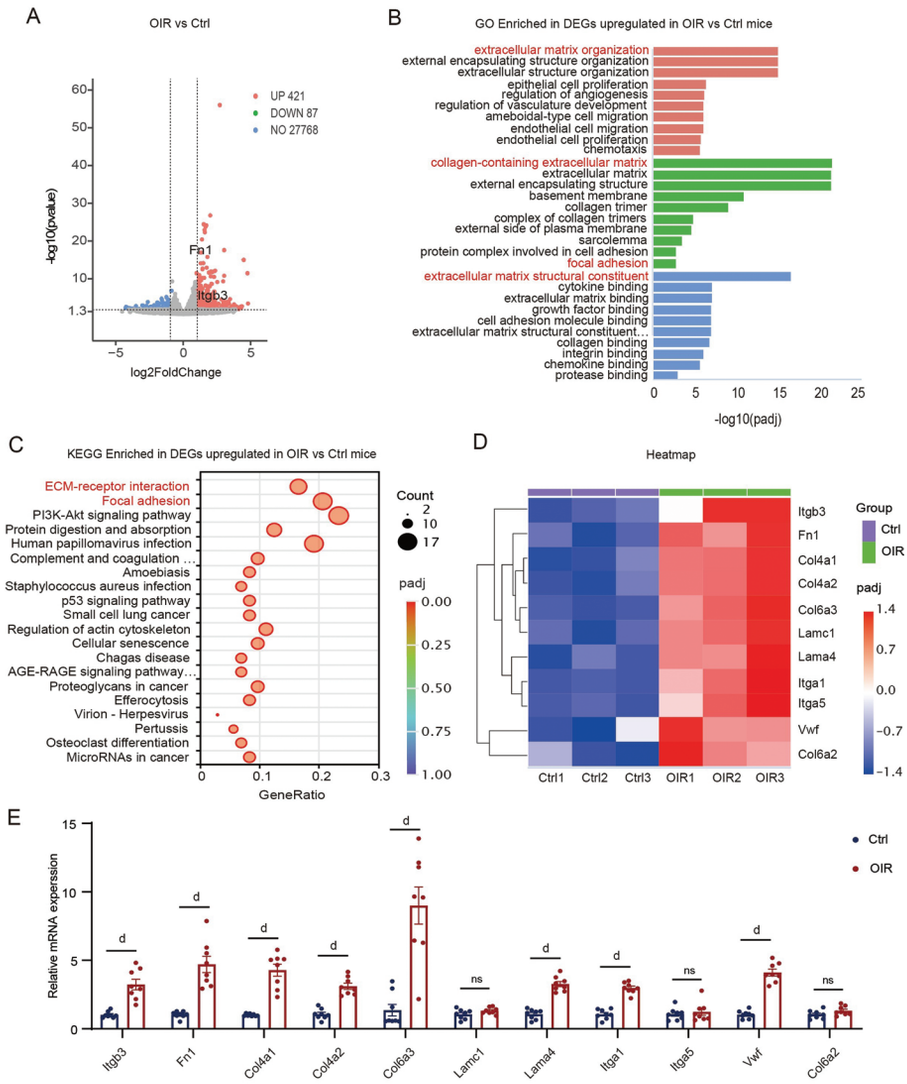


Figure 2 Transcriptomic profiling of OIR mouse retina identifies activation of ECM and FAK pathways Data are mean±SD. Statistical significance was determined by unpaired *t*-test: ^{d}P<0.0001; "ns" indicates not significant (P>0.05). A: Volcano plot of DEGs. Red and blue dots represent significantly upregulated and downregulated genes in OIR retinas compared to Ctrl, respectively (criteria: $|\log_2\text{FoldChange}|>1$, Padj<0.05). Key genes *Fn1* and *Itgb3* are labeled; B: Bar plot of GO functional enrichment analysis for upregulated DEGs in the OIR group; C: Bubble plot of KEGG pathway enrichment analysis for upregulated DEGs in the OIR group; D: Heatmap showing the expression of common DEGs shared between the KEGG "focal adhesion" and "ECM-receptor interaction" pathways; E: Validation of the expression of all DEGs shown in the heatmap (D) in both Ctrl and OIR retinal tissues by qRT-PCR (n=8 mice per group). OIR: Oxygen-induced retinopathy; ECM: Extracellular matrix; FAK: Focal adhesion; DEGs: Differentially expressed genes; Ctrl: Control; GO: Gene Ontology; KEGG: Kyoto Encyclopedia of Genes and Genomes; qRT-PCR: Quantitative reverse transcription polymerase chain reaction; SD: Standard deviation.

M2=0.897±0.048 (n=8 mice). These data confirm that ITGB3 is predominantly expressed on retinal blood vessels during pathological angiogenesis. qPCR analysis revealed elevated mRNA levels of pro-inflammatory cytokines (*iNOS*, *IL-1β*, *TNF-α*) and *IL-10* in OIR retinas, while *Arg1* was unchanged, indicating a pro-inflammatory microenvironment.

Hypoxic Microglia Promote Endothelial Cell Functions by Activating the ITGB3-FAK/Akt Pathway CM from Hyp-CM significantly increased the migration (wound closure rate) and tube-forming capacity of BEnd.3 endothelial cells compared to control medium or normoxic microglia CM (Ctrl-CM; Figure 4A–4F). Tube formation assays showed that Hyp-CM induced a dense and complex network. Quantitative analysis revealed that the number of nodes was significantly higher in the Hyp-CM group (499.0±45.5) than in Ctrl (195.0±49.4, P=0.0013) and Ctrl-CM (306.0±68.0, P=0.0123; Figure 4E). Similarly, the total branch length was significantly increased in Hyp-CM-treated cells (29 482±2833 μm) compared with Ctrl (15 861±1403 μm, P=0.0004) and Ctrl-CM (18 455±1226 μm, P=0.0011; Figure 4F). These data confirm that hypoxic microglial CM promotes endothelial tube formation.

At the molecular level, Hyp-CM specifically upregulated ITGB3 protein expression and elevated phosphorylation of

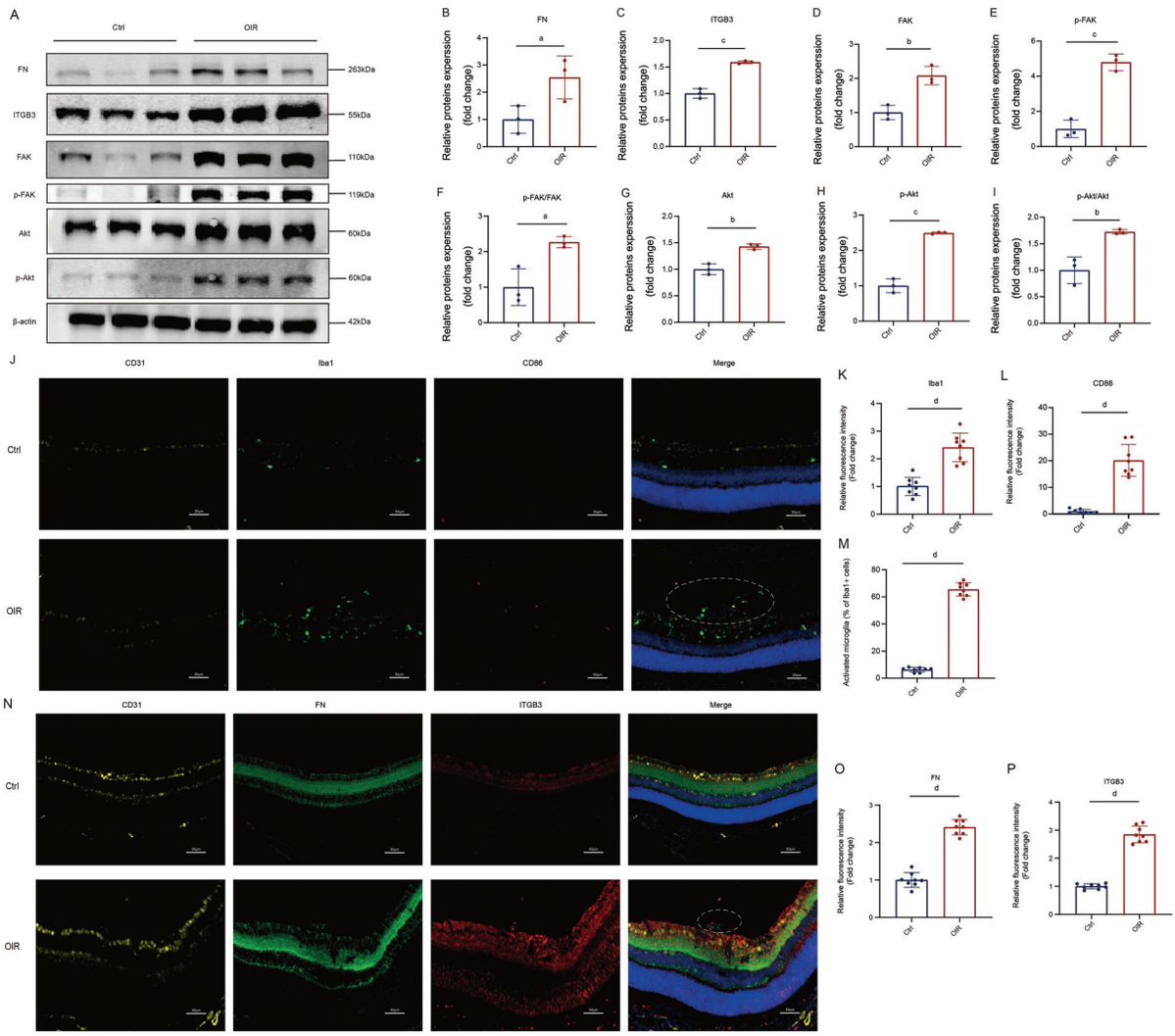


Figure 3 *In vivo* validation shows FN-ITGB3-FAK/Akt activation and co-localization with activated microglia Data are mean±SD. Statistical significance was determined by unpaired *t*-test: [a]*P*<0.05, [b]*P*<0.01, [c]*P*<0.001, [d]*P*<0.0001. A–I: Western blot analysis and quantification of the expression of FN, ITGB3, total FAK (FAK), phosphorylated FAK (p-FAK, Tyr397), total Akt (Akt), phosphorylated Akt (p-Akt, Ser473) in retinal tissues from Ctrl and OIR mice (*n*=3 independent biological replicates per group); J: Representative immunofluorescence co-staining images of retinal sections. Staining for CD31 (yellow), Iba1 (green), CD86 (red), and DAPI (blue). White dashed circles outline neovascular clusters breaching the internal limiting membrane in the OIR group. Scale bar: 50 μm; K, L: Quantitative analysis of the average fluorescence intensity for Iba1 (K) and CD86 (L) across the entire retinal sections, respectively (*n*=8 independent mice per group); M: Quantitative analysis of the proportion of activated (amoeboid) microglia among total Iba1+cells (*n*=8 independent mice per group, 4 fields per retina); N: Representative immunofluorescence co-staining images of retinal sections. Staining for CD31 (yellow), FN (green), ITGB3 (red), and DAPI (blue). White dashed circles outline areas in the OIR group where FN and ITGB3 signals show significant co-localization. Scale bar: 50 μm; O, P: Quantitative analysis of the average fluorescence intensity for FN (O) and ITGB3 (P) across the entire retinal sections, respectively (*n*=8 independent mice per group). FN: Fibronectin; ITGB3: Integrin β3; FAK: Focal adhesion kinase; Akt: Protein kinase B; Ctrl: Control; OIR: Oxygen-induced retinopathy; CD31: Platelet endothelial cell adhesion molecule-1; Iba1: Ionized calcium-binding adapter molecule 1; CD86: Cluster of differentiation 86; DAPI: 4′,6-diamidino-2-phenylindole; SD: Standard deviation.

FAK and Akt in endothelial cells (Figure 4G–4N). These data indicate hypoxic microglia, *via* their secretome, potently activate the ITGB3-FAK-Akt pathway in endothelial cells.

Pharmacological Inhibition of ITGB3 or FAK Attenuates the Pro-angiogenic Effects Exogenous FN protein mimicked the pro-migratory effects of Hyp-CM. Conversely, both the ITGB3 inhibitor cilengitide and the FAK inhibitor PF-573228 significantly attenuated the Hyp-CM-induced promotion of endothelial cell migration (Figure 5A–5B). Exogenous FN protein (Ctrl+FN) mimicked the pro-tubulogenic effect of Hyp-CM, increasing both the number of nodes (534.3±79.2, *P*=0.0015 *vs* Ctrl) and total branch length (Figure 5C–5E). The addition of cilengitide (Hyp-CM+Cil) or PF-573228 (Hyp-CM+PF) dramatically reduced Hyp-CM-induced node

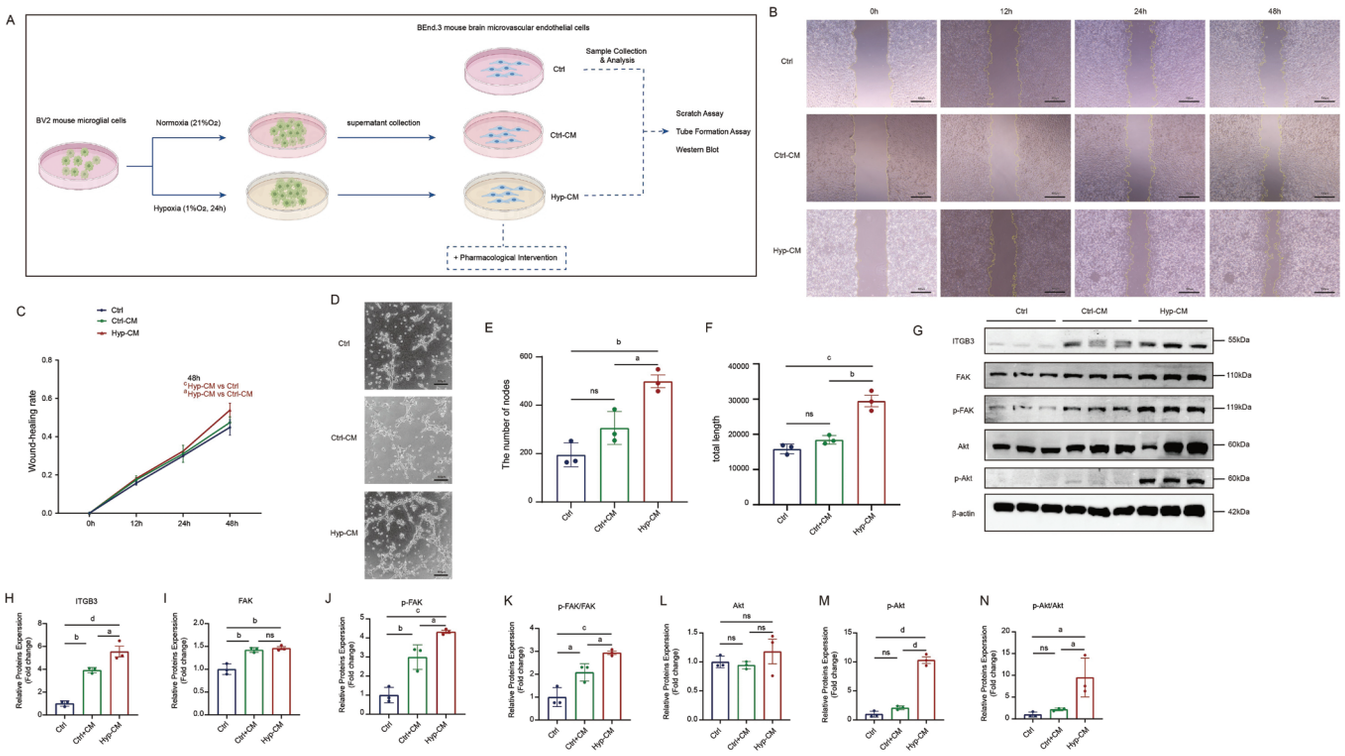


Figure 4 Hypoxic microglial conditioned medium promotes endothelial cell migration and tube formation *via* the ITGB3-FAK-Akt pathway

Data are mean±SD. Statistical significance was determined by one-way ANOVA with Tukey's post hoc test: [a]*P*<0.05, [b]*P*<0.01, [c]*P*<0.001, [d]*P*<0.0001; "ns" indicates not significant. A: Schematic flowchart of the *in vitro* mechanistic study (created with Figdraw); B: Representative images of the scratch wound healing assay of mouse BEnd.3 treated with different conditioned media at 0, 12, 24, and 48h. Yellow dashed lines indicate the boundaries of the wound (cell-free) areas. Groups: Ctrl (control medium), Ctrl-CM (conditioned medium from normoxic microglia), Hyp-CM (conditioned medium from hypoxic microglia). Scale bar: 500 μm; C: Quantitative analysis of the wound healing rate (*n*=3 independent experiments). The wound healing rate was calculated as: (initial wound area-unhealed area at the indicated time point)/initial wound area×100%; D: Representative images (10-fold) of the endothelial tube formation assay. Scale bar: 100 μm; E: Quantification of the number of nodes in tube formation networks (*n*=3 independent experiments); F: Quantification of total branch length (Tot. length) in tube formation networks (*n*=3 independent experiments); G–N: Western blot analysis and quantification of the expression of ITGB3, FAK, p-FAK (Tyr397), Akt, p-Akt (Ser473) in endothelial cells treated with different conditioned media (*n*=3 independent experiments). BEnd.3: Brain microvascular endothelial cells; Ctrl: Control medium; Ctrl-CM: Conditioned medium from normoxic microglia; Hyp-CM: Conditioned medium from hypoxic microglia; ITGB3: Integrin β3; FAK: Focal adhesion kinase; Akt: Protein kinase B; ANOVA: One-way analysis of variance; SD: Standard deviation.

formation (Figure 5D) and total branch length (Figure 5E), with both inhibitors bringing the values below those of Ctrl (*P*<0.0001 for all comparisons). No significant difference was observed between the two inhibitor groups. These results demonstrate that the FN–ITGB3–FAK axis is functionally required for the pro-angiogenic activity of Hyp-CM.

Western blot analysis showed exogenous FN increased ITGB3 expression and FAK/Akt phosphorylation. Cilengitide not only suppressed the Hyp-CM-induced up-regulation of ITGB3 but also blocked FAK and Akt activation. PF-573228, while reducing FAK phosphorylation, also inhibited Hyp-CM-induced ITGB3 upregulation and Akt activation (Figure 5F–5M). These results establish the functional necessity of the FN-ITGB3-FAK axis in mediating the pro-angiogenic effects of hypoxic microglia.

VEGF Partially Contributes to Hyp-CM-induced Endothelial Migration To determine whether VEGF mediates the pro-migratory activity of Hyp-CM, we performed scratch wound healing assays in the presence of a neutralizing anti-VEGF antibody (Figure 6A, 6B). The antibody's neutralizing capacity was validated by the rmVEGF+αVEGF group, which showed no significant difference from the Ctrl group at 24h and 48h, confirming effective blockade of exogenous VEGF. Hyp-CM significantly promoted wound closure compared to Ctrl at 24h and 48h. Addition of the anti-VEGF antibody significantly reduced migration relative to Hyp-CM at 48h, but the residual migration remained significantly higher than in the Ctrl group. The isotype control IgG had no effect. These data indicate that while VEGF contributes partially, a substantial VEGF-independent

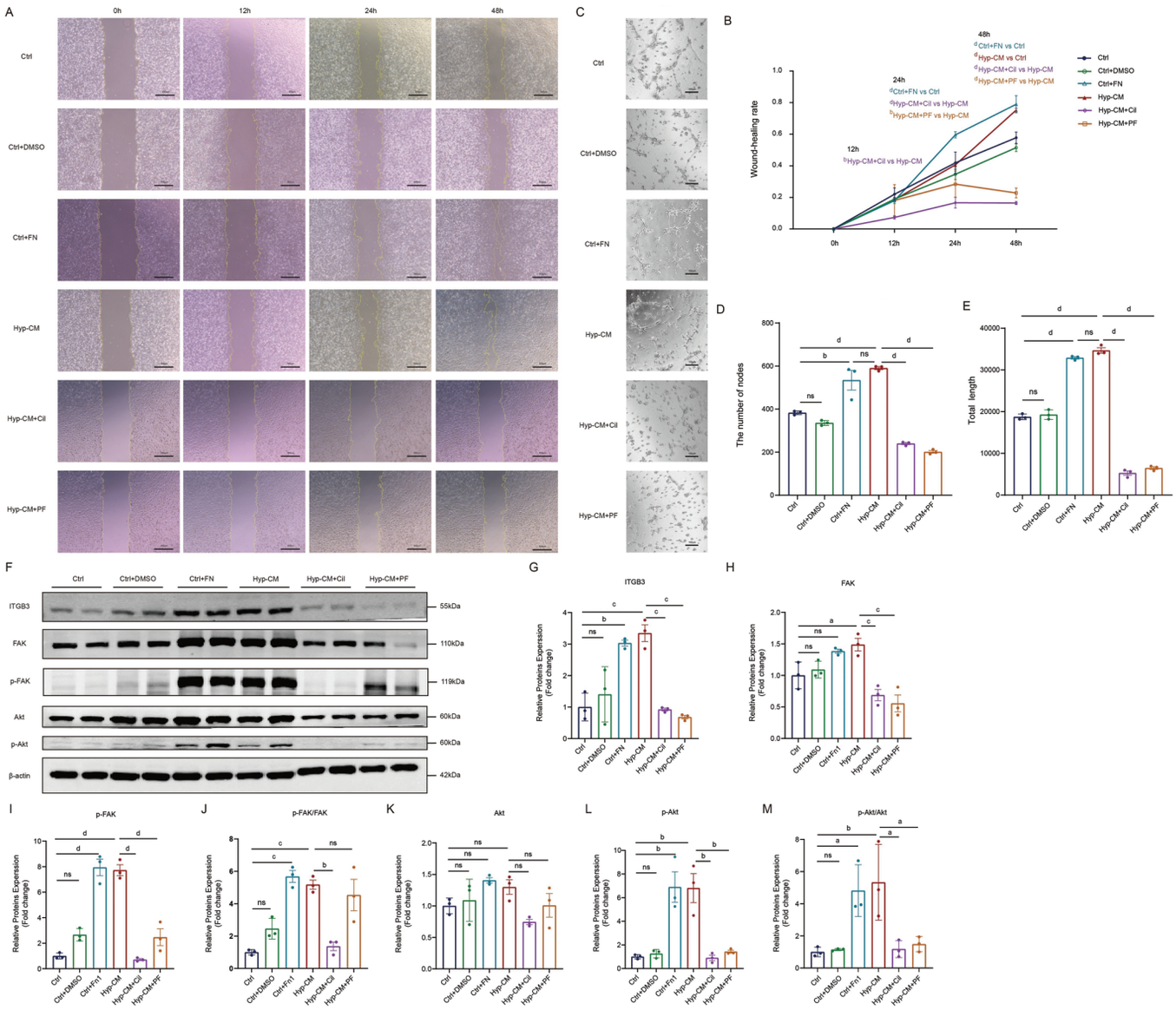


Figure 5 Pharmacological inhibition of integrin ITGB3 or FAK abolishes the pro-angiogenic effects of hypoxic microglial conditioned medium Data are mean±SD. Statistical significance was determined by one-way ANOVA with Tukey's post hoc test. [a]*P*<0.05, [b]*P*<0.01, [c]*P*<0.001, [d]*P*<0.0001; "ns" indicates not significant. A: Representative images of the scratch wound healing assay of mouse BEnd.3 under different treatments at 0, 12, 24, and 48h. Yellow dashed lines indicate the boundaries of the wound (cell-free) areas. Groups: Ctrl (control medium), Ctrl+DMSO (control medium with DMSO vehicle), Ctrl+FN (control medium with exogenous FN protein), Hyp-CM (conditioned medium from hypoxic microglia), Hyp-CM+Cil (Hyp-CM with the αvβ3/αvβ5 integrin inhibitor Cilengitide), Hyp-CM+PF (Hyp-CM with the FAK inhibitor PF-573228). Scale bar: 500 μm; B: Quantitative analysis of the wound healing rate (*n*=3 independent experiments); C: Representative images (10-fold) of the endothelial tube formation assay under different treatments. Group order is the same as in (A). Scale bar: 100 μm; D: Quantification of the number of nodes in tube formation networks (*n*=3 independent experiments); E: Quantification of total branch length (Tot. length) in tube formation networks (*n*=3 independent experiments); F–M: Western blot analysis and quantification of the expression of ITGB3, FAK, p-FAK (Tyr397), Akt, p-Akt (Ser473) in endothelial cells under different treatments (*n*=3 independent experiments). ITGB3: Integrin β3; FAK: Focal adhesion kinase; BEnd.3: Brain microvascular endothelial cells; Ctrl: Control medium; DMSO: Dimethyl sulfoxide; FN: Fibronectin; Hyp-CM: Conditioned medium from hypoxic microglia; Cil: Cilengitide (β3 integrin inhibitor); PF: PF-573228 (FAK inhibitor); Akt: Protein kinase B; SD: Standard deviation; ANOVA: One-way analysis of variance.

component persists in Hyp-CM-induced endothelial migration. Tube formation assays further confirmed the partial contribution of VEGF. Hyp-CM significantly increased the number of nodes (581.3±12.0) and total branch length (36 251±596 μm; Figure 6C–6E). Addition of the anti-VEGF antibody significantly reduced node number (490.0±14.1) and total branch length (27 309±2029 μm). However, both parameters remained significantly higher than in the Ctrl

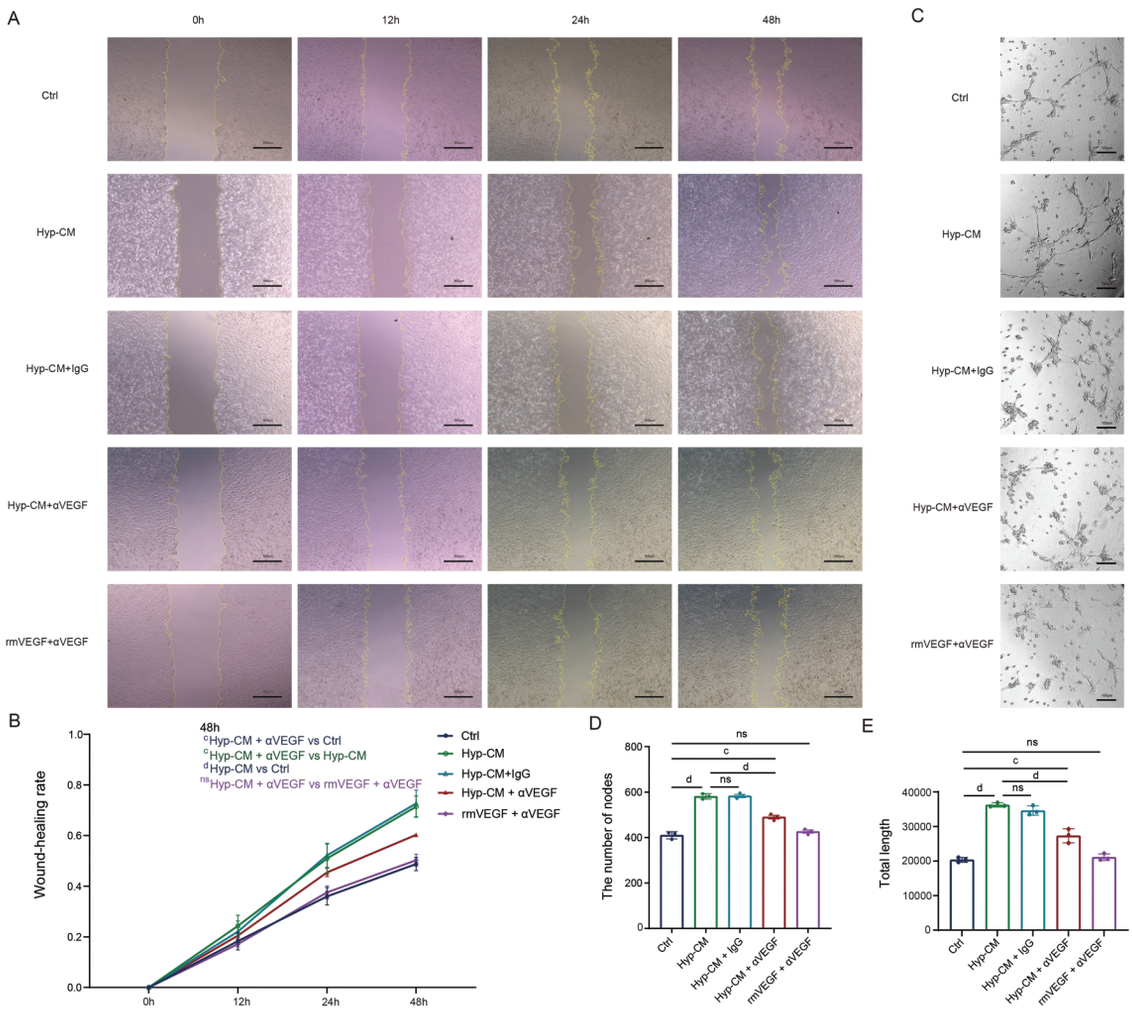


Figure 6 VEGF partially contributes to the pro-angiogenic effect of hypoxic microglial conditioned medium Data are mean±SD. Statistical significance was determined by one-way ANOVA with Tukey's post hoc test. $^{c}P<0.001$, $^{d}P<0.0001$; "ns" indicates not significant. A: Representative images of the scratch wound healing assay of mouse BEnd.3 under different treatments at 0, 12, 24, and 48h. Yellow dashed lines indicate the boundaries of the wound (cell-free) areas. Groups: Ctrl (control medium), Hyp-CM (conditioned medium from hypoxic microglia), Hyp-CM+IgG (control medium with IgG vehicle), Hyp-CM+αVEGF (control medium with anti-mouse VEGF antibody), αVEGF+rmVEGF (recombinant mouse VEGF with anti-mouse VEGF antibody). Scale bar: 500 μm; B: Quantitative analysis of the wound healing rate (*n*=3 independent experiments); C: Representative images (10-fold) of the endothelial tube formation assay under different treatments. Group order is the same as in A. Scale bar: 100 μm; D: Quantification of the number of nodes in tube formation networks (*n*=3 independent experiments); E: Quantification of total branch length (Tot. length) in tube formation networks (*n*=3 independent experiments). VEGF: Vascular endothelial growth factor; SD: Standard deviation; ANOVA: One-way analysis of variance; BEnd.3: Brain microvascular endothelial cells; Ctrl: Control medium; Hyp-CM: Conditioned medium from hypoxic microglia; IgG: Immunoglobulin G; αVEGF: Anti-mouse VEGF antibody; rmVEGF: Recombinant mouse VEGF Protein.

group. The isotype control IgG had no effect, and the positive control (rmVEGF+αVEGF) showed no significant difference from Ctrl, confirming effective neutralization of exogenous VEGF. These data indicate that while VEGF contributes partially, a substantial VEGF-independent component persists in Hyp-CM-induced tube formation.

***In vivo* Cilengitide Treatment Reduces Pathological Neovascularization in OIR** To evaluate the therapeutic potential of ITGB3 inhibition *in vivo*, we performed intravitreal injection of cilengitide in OIR mice (Figure 7A). Representative CD31-stained retinal flat mounts are shown in Figure 7B. Quantitative analysis revealed that the RNV area, expressed as a percentage of total retinal area, was significantly lower in the cilengitide-treated group (0.721%±0.207%) compared to the IgG control group (1.975%±0.164%; $P<0.0001$; Figure 7C). These data confirm that pharmacological inhibition of ITGB3 effectively suppresses pathological angiogenesis in the OIR model.

DISCUSSION

This study defines a novel pathway that operates in parallel

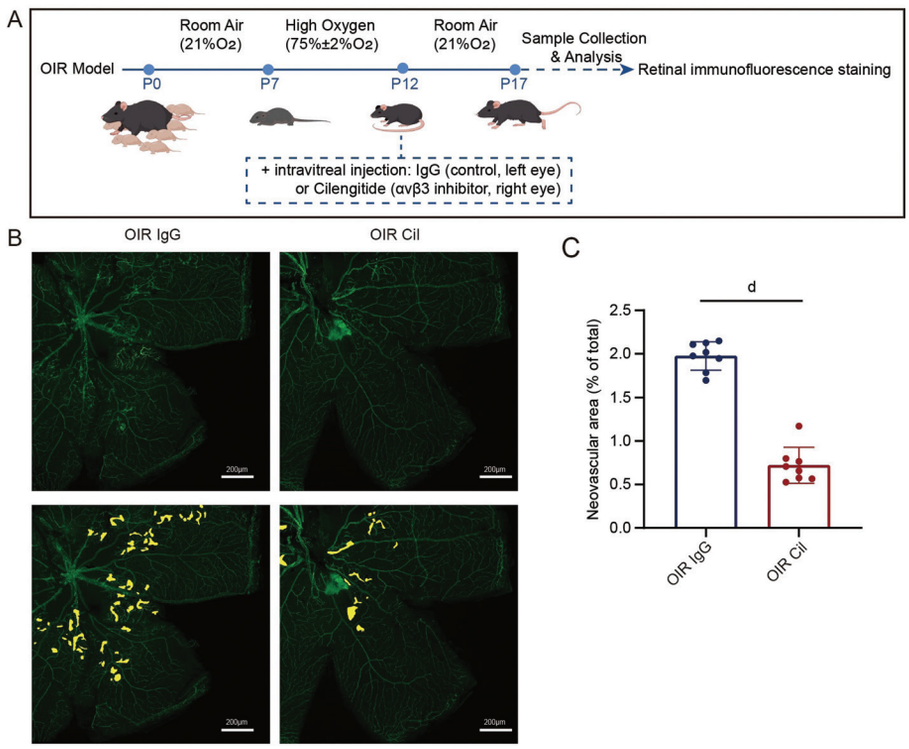


Figure 7 Intravitreal cilengitide reduces pathological neovascularization in the OIR model Data are mean±SD. Statistical significance was determined by unpaired *t*-test: $^{d}P<0.0001$. A: Schematic timeline of OIR induction and intravitreal injection; B: Representative CD31-stained retinal flat mounts from OIR mice injected with isotype control IgG (left) or cilengitide (right). Neovascular areas are outlined in yellow. Scale bar: 200 μm; C: Quantification of neovascular area as a percentage of total retinal area (*n*=8 eyes per group). OIR: Oxygen-induced retinopathy; P: Postnatal day; CD31: Platelet endothelial cell adhesion molecule-1; SD: Standard deviation; IgG: Immunoglobulin G.

with VEGF signaling to drive pathological angiogenesis in ischemic retinopathy. We demonstrate that hypoxia-activated microglia are associated with FN upregulation, and that the FN/ITGB3/FAK/Akt signaling axis plays a key role in promoting pathological angiogenesis. This, in turn, activates the ITGB3-FAK/Akt signaling axis in endothelial cells, promoting their migration and tube formation—a cascade effectively disrupted by integrin or FAK inhibition. Our findings thus integrate immune activation, ECM mechanics, and intracellular signaling into a coherent "hypoxia–microglia–ECM–integrin" axis, offering a mechanistic explanation for anti-VEGF resistant neovascularization.

The OIR model reliably recapitulates the vaso-obliteration and pathological neovascularization seen in human ischemic retinopathies[12]. In the OIR model, the avascular area is a well-established readout of ischemia-induced vaso-obliteration, which is the primary driver of subsequent pathological neovascularization[14]. Therefore, we used avascular area as a complementary endpoint alongside direct quantification of neovascular tufts. While the HIF–VEGF axis is central, the prevalent issue of anti-VEGF therapy resistance underscores the necessity to identify alternative pathways[3-5]. Our transcriptomic data provide systematic evidence for the global activation of ECM and focal adhesion pathways in OIR, pointing to a potent angiogenic driver that operates in parallel with VEGF.

Within the dysregulated neurovascular unit, microglia are key sentinels and modulators. Their activation and co-localization with neovessels in OIR align with their pro-angiogenic role[6]. We show that microglial activation is associated with ECM remodeling, with FN as a key component. FN upregulation marks a shift of the microenvironment from a passive scaffold to a dynamic signaling platform[2]. FN engages ITGB3, a receptor with established roles in angiogenesis[9,15-17] and mechanosensing[18-19]. The co-localization of FN/ITGB3 with activated microglia and neovessels *in vivo*, together with the pro-angiogenic effect of hypoxic microglial CM *in vitro*, establishes a functional link. This aligns with evidence that FN upregulates ITGB3 and activates downstream signaling in other contexts[20-22]. Moreover, the upregulation of tumor necrosis factor-alpha (TNF-α), interleukin-1 beta (IL-1β), and inducible nitric oxide synthase (iNOS) in OIR retinas confirms the presence of a pro-inflammatory microenvironment, a recognized hallmark of ischemic retinopathies such as diabetic retinopathy[23]. This hypoxia-driven neuroinflammation leading to ECM remodeling and neurovascular dysfunction is also observed in cerebral small vessel disease[24], underscoring the broad relevance of this axis. We note that our data

primarily support ITGB3-associated signaling; definitive αvβ3 heterodimer involvement and exclusion of other FN-binding integrins (*e.g.*, α5β1) require further study.

Activation of downstream FAK/Akt confirms signal transduction through this axis. Pharmacological inhibition not only blocks downstream phosphorylation but also suppresses upstream ITGB3 upregulation, suggesting a positive feedback loop that may sustain pathway activation and contribute to therapeutic resistance. The use of microglial CM is a well-accepted approach to study microglia-endothelial paracrine signaling[25-27], although CM recapitulates soluble signals rather than the full native ECM. Other soluble factors may also contribute.

Our VEGF neutralization experiments showed that an anti-VEGF antibody only partially reduced Hyp-CM effects, leaving a significant residual activity that was completely blocked by integrin/FAK inhibition (Figures 5–6). Thus, the FN/ITGB3/FAK/Akt axis can promote angiogenesis independently of VEGF. These two pathways may synergize under hypoxia, and while anti-VEGF therapy blocks one major route, the persistent FN-integrin signaling could drive resistance. These findings support the concept that the FN/ITGB3/FAK/Akt axis operates in parallel with VEGF signaling, and dual targeting of both pathways may offer a more effective strategy for ischemic retinopathies.

The most significant translational implication of our study lies in the validation of this axis as a druggable target. Intravitreal injection of Cilengitide, an integrin αvβ3/αvβ5 inhibitor, markedly reduced the neovascular area in OIR mice (Figure 7), providing direct *in vivo* evidence of therapeutic efficacy. This aligns with the *in vitro* observation that Cilengitide completely reverses hypoxic microglial effects (Figure 5). Cilengitide, a cyclic RGD peptide, has been evaluated in clinical trials for cancer[28], including a phase I trial combining it with a VEGFR inhibitor in recurrent glioblastoma underscores the active clinical interest in co-targeting VEGF and integrin pathways[29]. This is highly relevant as integrin antagonists are recognized emerging therapeutic opportunities[30-31], with agents like Risuteganib and Luminate already under clinical investigation for retinal vascular diseases[32-33]. Similarly, FAK inhibition proved equally effective. Therefore, our data provide a strong preclinical rationale for repurposing or developing integrin/FAK-targeted therapies to overcome anti-VEGF resistance, either as monotherapy or—more pertinently—in combination with anti-VEGF agents[34]. This combination strategy, which targets both a soluble growth factor (VEGF) and a mechano-sensitive adhesion pathway (integrin/FAK), is particularly compelling given the multifaceted nature of clinical resistance. Notably, in diseases such as neovascular age-related macular degeneration, incomplete response to anti-VEGF therapy is characterized not only by persistent leakage but also by lesion fibrosis and arteriolarization—features directly linked to ECM remodeling and mesenchymal activation. Thus, simultaneously inhibiting VEGF and the ECM–integrin axis may address a broader spectrum of pathological processes. This approach is further supported by recent evidence that melatonin inhibits OIR neovascularization through dual targeting of FN1 and VEGFR2[35].

This study has limitations that point to future research directions. First, the precise cellular source of FN in the OIR retina—whether microglia, astrocytes, endothelial cells, or other glial cells—remains unknown, and the specific microglial-derived factors driving FN upregulation have not been identified. Future studies using microglia-specific FN knockout, pharmacological microglia depletion, or unbiased secretomic profiling of Hyp-CM will be required to establish a definitive causal link between microglia and ECM remodeling. Second, while published evidence supports the presence of FN in human proliferative diabetic retinopathy (PDR) tissues and the existence of a pro-angiogenic microglial subset[36-37], direct validation of this signaling axis in human retinal samples from PDR or ROP patients would further strengthen its clinical relevance.

In summary, we have delineated a complete pathogenic circuit in which hypoxia-driven microglial activation is associated with ECM remodeling, leading to sustained activation of endothelial ITGB3-FAK/Akt signaling and pathological angiogenesis. By moving beyond the VEGF-centric paradigm, this work identifies the "hypoxia–microglia–ECM–integrin" axis as a novel and therapeutically targetable mechanism contributing to anti-VEGF resistance, providing a concrete strategy for next-generation therapy development in ischemic retinopathies.

ACKNOWLEDGEMENTS

Authors' Contributions: Zhu SQ conceived and designed the study, and acquired funding; Hao LC performed the experiments, collected data, and wrote the original draft; Li DH and Zhang K provided technical support and performed data analysis; Liu CZ and Sun MH critically revised the manuscript; Gao XX contributed to study conception and critically reviewed the manuscript.

Data Availability Statement: The data supporting the findings of this study are available within the article. The RNA sequencing data generated in this study have been deposited in the NCBI Sequence Read Archive (SRA) under BioProject accession number PRJNA1390860 (https://www.ncbi.nlm.nih.gov/bioproject/PRJNA1390860).

AI-Generated Content Disclosure: The authors declare that no generative artificial intelligence (AI) or AI-assisted technologies were used in the preparation of this manuscript.

Foundations: Supported by the National Natural Science Foundation of China (No.52273134; No.52073181).

Conflicts of Interest: Hao LC, None; **Li DH,** None; **Zhang K,** None; **Liu CZ,** None; **Sun MH,** None; **Gao XX,** None; **Zhu SQ,** None.

REFERENCES

1 Fevereiro-Martins M, Marques-Neves C, Guimarães H, *et al*. Retinopathy of prematurity: a review of pathophysiology and signaling pathways. *Surv Ophthalmol* 2023;68(2):175-210.

2 Hu AY, Schmidt MHH, Heinig N. Microglia in retinal angiogenesis and diabetic retinopathy. *Angiogenesis* 2024;27(3):311-331.

3 Mettu PS, Allingham MJ, Cousins SW. Incomplete response to Anti-VEGF therapy in neovascular AMD: exploring disease mechanisms and therapeutic opportunities. *Prog Retin Eye Res* 2021;82:100906.

4 Yang SQ, Zhao JK, Sun XD. Resistance to anti-VEGF therapy in neovascular age-related macular degeneration: a comprehensive review. *Drug Des Dev Ther* 2016;10:1857-1867.

5 Maguire MG, Martin DF, Ying GS, *et al*. Five-year outcomes with anti–vascular endothelial growth factor treatment of neovascular age-related macular degeneration. *Ophthalmology* 2016;123(8):1751-1761.

6 Boeck M, Thien A, Wolf J, *et al*. Temporospatial distribution and transcriptional profile of retinal microglia in the oxygen-induced retinopathy mouse model. *Glia* 2020;68(9):1859-1873.

7 Crapser JD, Arreola MA, Tsourmas KI, *et al*. Microglia as hackers of the matrix: sculpting synapses and the extracellular space. *Cell Mol Immunol* 2021;18(11):2472-2488.

8 Meldolesi J. Pharmacology of the cell/matrix form of adhesion. *Pharmacol Res* 2016;107:430-436.

9 Zoppi N, Chiarelli N, Ritelli M, *et al*. Multifaced roles of the αvβ3 integrin in ehlers–danlos and arterial tortuosity syndromes' dermal fibroblasts. *Int J Mol Sci* 2018;19(4):982.

10 Pouw AE, Greiner MA, Coussa RG, *et al*. Cell-matrix interactions in the eye: from cornea to choroid. *Cells* 2021;10(3):687.

11 Irnaten M, Gaynor E, O'Brien C. The role of αvβ3 integrin in lamina cribrosa cell mechanotransduction in glaucoma. *Cells* 2024;13(17):1487.

12 Smith L, Wesolowski E, McLellan A, *et al*. Oxygen-induced retinopathy in the mouse. *Invest Ophthalmol Vis Sci* 1994;35(1):101-111.

13 Maurya M, Liu CH, Bora K, *et al*. Animal models of retinopathy of prematurity: advances and metabolic regulators. *Biomedicines* 2024;12(9):1937.

14 Connor KM, Krah NM, Dennison RJ, *et al*. Quantification of oxygen-induced retinopathy in the mouse: a model of vessel loss, vessel regrowth and pathological angiogenesis. *Nat Protoc* 2009;4(11):1565-1573.

15 Yang TL, Lee PL, Lee DY, *et al*. Differential regulations of fibronectin and laminin in Smad2 activation in vascular endothelial cells in response to disturbed flow. *J Biomed Sci* 2018;25(1):1.

16 Li YB, Yarahmadov T, Jahnke L, *et al*. Rho-kinase inhibition reduces subretinal fibrosis. *Cell Death Discov* 2025;11(1):428.

17 Gu YL, Dong BQ, He X, *et al*. The challenges and opportunities of αvβ3-based therapeutics in cancer: from bench to clinical trials. *Pharmacol Res* 2023;189:106694.

18 Benito-Jardón M, Klapproth S, Gimeno-LLuch I, *et al*. The fibronectin synergy site re-enforces cell adhesion and mediates a crosstalk between integrin classes. *eLife* 2017;6:e22264.

19 Zhuo PM, Li QH, Yang BS, *et al*. Interaction of integrin $\alpha_v\beta_3$ and fibronectin under fluid shear forces: implications for tumor cell adhesion and migration. *Front Cell Dev Biol* 2025;13:1512672.

20 Wareham LK, Calkins DJ. Making tracks: microglia and the extracellular matrix. *Mol Neurodegener* 2025;20(1):101.

21 Wu JL, Xu CF, Yang XH, *et al*. Fibronectin promotes tumor progression through integrin αvβ3/PI3K/AKT/SOX2 signaling in non-small cell lung cancer. *Heliyon* 2023;9(9):e20185.

22 Soriano AA, de Cristofaro T, di Palma T, *et al*. PAX8 expression in high-grade serous ovarian cancer positively regulates attachment to ECM *via* Integrin β3. *Cancer Cell Int* 2019;19:303.

23 Tang L, Xu GT, Zhang JF. Inflammation in diabetic retinopathy: possible roles in pathogenesis and potential implications for therapy. *Neural Regen Res* 2023;18(5):976-982.

24 Rosenberg GA. Extracellular matrix inflammation in vascular cognitive impairment and dementia. *Clin Sci* 2017;131(6):425-437.

25 Rymo SF, Gerhardt H, Wolfhagen Sand F, *et al*. A two-way communication between microglial cells and angiogenic sprouts regulates angiogenesis in aortic ring cultures. *PLoS One* 2011;6(1):e15846.

26 Yin J, Xu WQ, Ye MX, *et al*. Up-regulated basigin-2 in microglia induced by hypoxia promotes retinal angiogenesis. *J Cell Mol Med* 2017;21(12):3467-3480.

27 Bai Q, Wang X, Yan HX, *et al*. Microglia-derived Spp1 promotes pathological retinal neovascularization *via* activating endothelial kit/Akt/mTOR signaling. *J Pers Med* 2023;13(1):146.

28 Slack RJ, MacDonald SJF, Roper JA, *et al*. Emerging therapeutic opportunities for integrin inhibitors. *Nat Rev Drug Discov* 2022;21(1):60-78.

29 Gerstner ER, Ye XB, Duda DG, *et al*. A phase I study of cediranib in combination with cilengitide in patients with recurrent glioblastoma. *Neuro Oncol* 2015;17(10):1386-1392.

30 Chauhan MZ, Rather PA, Samarah SM, *et al*. Current and novel therapeutic approaches for treatment of diabetic macular edema. *Cells* 2022;11(12):1950.

31 Le Du J, Ronco C. Therapeutic strategies targeting ocular vasculopathies: current advances and emerging challenges. *Drug Discov Today* 2025;30(11):104496.

32 Shaw LT, Mackin A, Shah R, *et al*. Risuteganib-a novel integrin inhibitor for the treatment of non-exudative (dry) age-related macular degeneration and diabetic macular edema. *Exp Opin Invest Drugs* 2020;29(6):547-554.

33 van Hove I, Hu TT, Beets K, *et al*. Targeting RGD-binding integrins as an integrative therapy for diabetic retinopathy and neovascular age-related macular degeneration. *Prog Retin Eye Res* 2021;85:100966.

34 Campochiaro PA, Akhlaq A. Sustained suppression of VEGF for treatment of retinal/choroidal vascular diseases. *Prog Retin Eye Res* 2021;83:100921.

35 Chen F, Yang X, Yin YW, *et al*. Melatonin alleviates retina angiogenesis by targeting fibronectin and the VEGF pathway. *FASEB J* 2025;39(19):e71073.

36 Wei QL, Zhang T, Jiang R, *et al*. Vitreous fibronectin and fibrinogen expression increased in eyes with proliferative diabetic retinopathy after intravitreal anti-VEGF therapy. *Invest Ophthalmol Vis Sci* 2017;58(13):5783-5791.

37 Zou KY, Li X, Ren BB, *et al*. Single-cell analysis identifies MKI67+ microglia as drivers of neovascularization in proliferative diabetic retinopathy. *J Transl Med* 2025;23(1):310.